RSC Advances

PAPER

View Article Online
View Journal | View Issue

Cite this: *RSC Adv.*, 2022, **12**, 16444

A sustained-release Trametinib bio-multifunction hydrogel inhibits orthodontically induced inflammatory root resorption†

Hang Yu,[ab] Zhina Wu,[ab] Xingfu Bao,[ab] Xiaoduo Tang,‡*[cd] Junhu Zhang,*[cd] Yi Zhang‡*[ab] and Min Hu‡*[ab]

Orthodontic tooth movement (OTM) is a bone reconstruction process. In most cases, OTM could induce root resorption as a common side effect, called orthodontically induced inflammatory root resorption (OIIRR). OIIRR affects tooth health and interferes with the stability of orthodontic treatment. Osteoclasts, which perform bone resorption in OTM, attack cementum, causing OIIRR. Many signaling pathways are involved in the maturation and differentiation of osteoclasts, among which the ERK1/2 is one of the important pathways. In this experiment, we added Trametinib (Tra), a specific inhibitor of ERK1/2, to catechol-modified chitosan (CHI-C) and oxidized dextran (ODex) to form a CCOD–Trametinib composite hydrogel (CCOD–Tra) to prevent OIIRR. CCOD–Tra exhibited good biocompatibility, injectability, strong adhesion, good hemostatic function and sustained release of Tra. We performed local injection of CCOD–Tra into the periodontal tissues of rats. CCOD–Tra firmly adhered to the periodontal tissues and then released Tra to establish a good biological environment and maintain a drug concentration at a high level around the roots for a long time. H&E, TRAP, immunochemistry staining and micro-CT indicated that CCOD–Tra had a good effect in terms of preventing OIIRR. Cell experiments showed that CCOD–Tra reduced the expression of TRAP, MMP-9 and C-FOS in osteoclast cells through the ERK1/2 signaling pathway to inhibit the differentiation and maturation of osteoclasts. Based on the above results, we concluded that CCOD–Tra had the ability to prevent OIIRR, the high adhesion and injectability of CCOD may provide better therapeutic ideas for clinical prevention of OIIRR.

Received 5th February 2022
Accepted 13th May 2022

DOI: 10.1039/d2ra00763k

rsc.li/rsc-advances

1. Introduction

With societal development and improved awareness of oral health, an increasing number of people are choosing orthodontic treatment. The inevitable complications in orthodontic treatment have become a focus of concern for orthodontists and patients. Orthodontic tooth movement (OTM) is a process of alveolar bone remodeling stimulated by force.[1,2] During OTM, the damage of cementum and dentin is called orthodontically induced inflammatory root resorption (OIIRR), OIIRR leads to root shortening and causes tooth loss, which is an inevitable side effect of OTM.[3] Approximately 90% of orthodontic patients will experience OIIRR.[4–6] Therefore, preventing OIIRR is still a challenge for orthodontists.

During orthodontic tooth movement, osteoclasts are the key factor affecting alveolar bone resorption, but they also attack the cementum adjacent to the hyalinized area of the periodontal ligament, causing OIIRR.[7,8] The differentiation of osteoclast is triggered by receptor activator of nuclear factor kappa B ligand (RANKL) binds to receptor activator of nuclear factor kappa B (RANK).[9–11] When RANKL binds to RANK, the intracellular domain of RANK will activate many downstream pathways.[12–14] Many studies have shown that extracellular regulated protein kinases 1/2 (ERK1/2) signaling is one of the most important pathways mediate osteoclast differentiation,[15–17] when ERK1/2 pathway is activated, it promotes the expression of many osteoclast-related cytokines, such as tartrate resistant acid phosphatase (TRAP), c-fos and matrix metalloprotein-9 (MMP-9), which are closely related to the osteoclast differentiation and bone resorption.[18–20] In terms of preventing root resorption, scholars had found that blocking the ERK1/2 pathway can reduce the occurrence of root resorption.[21] Therefore, ERK1/2 could be used as an important target

[a]*Department of Orthodontics, Hospital of Stomatology, Jilin University, No. 1500 Qinghua Road, ChaoYang District, Changchun, Jilin, P. R. China. E-mail: zhangyi0519@jlu.edu.cn; Fax: +86 431 88975348; Tel: +86 431 85579371; +86 13504484365*

[b]*Jilin Provincial Key Laboratory of Tooth Development and Bone Remodeling (School and Hospital of Stomatology, Jilin University), P. R. China*

[c]*State Key Laboratory of Supramolecular Structure and Materials, College of Chemistry, Jilin University, Changchun 130012, P. R. China*

[d]*Joint Laboratory of Opto-Functional Theranostics in Medicine and Chemistry, The First Hospital of Jilin University, Changchun 130021, P. R. China*

† Electronic supplementary information (ESI) available. See https://doi.org/10.1039/d2ra00763k

‡ This work is also co-corresponding to Min Hu, Xiaoduo Tang and Yi Zhang.

to prevent root resorption. Trametinib (Tra, GSK1120212) is a highly selective inhibitor of ERK1/2 pathway,[22,23] which has been proven to have anti-inflammatory properties and improve rheumatoid arthritis symptoms and has been used in some bone treatment applications,[24,25] therefore, in this experiment, we chose Tra to prevent OIIRR by local injection. In order to improve the local therapeutic effect of Tra, we consider wrapping Tra with biomaterials so that it can stay in the periodontal tissue and sustained-release drugs for a long time. Currently, many biomaterials have been used as delivery agents for local periodontal treatment, such as sponges, electrospun nanocellulose membranes, hydrogels, and nanofiber mats.[26–31] Among them, hydrogel polymers have been one of the most popular drug delivery biomaterials because of their ability to design gel biological functions according to drug delivery requirements.[32–35]

Based on previous works,[36] we synthesized dopamine-modified chitosan (CHI-C) and aldehyde-modified dextran (ODex) and blended them using amide bonds as the gel forming mechanism to synthesize a biomultifunctional hydrogel (CCOD) for skin repair. In this work, we took advantage of the biological versatility of this gel, encapsulated Tra in the gel (CCOD–Tra), locally injected CCOD–Tra into the rats' periodontal area, CCOD–Tra adhered to the local periodontal tissue and effectively inhibit OIIRR. *In vitro* experiments we proved that CCOD–Tra inhibited the differentiation of osteoclasts by blocking the ERK1/2 signaling pathway. Therefore, ERK1/2 could be considered as a target for clinical treatment to prevent OIIRR and CCOD was a biological carrier that improved the effect of local periodontal treatment, which provided a new direction for clinical treatment.

2. Materials and methods

2.1 Materials and reagents

Chitosan, 3,4-dihydroxy hydrocinnamic acid, 1-ethyl-3-(3-dimethylamino-propyl)-carbodiimide hydrochloride (EDC), and dextran were purchased from Aladdin Reagents. Sodium periodate ($NaIO_4$) was purchased from Acros. Trametinib was purchased from Selleck. The TRAP staining kit was purchased from Wako. The RNA extraction kit was purchased from Chengdu Forge Biotechnology Co., Ltd. (China). HiFiScript gDNA Removal RT MasterMix and MagicSYBR Mixture were purchased from Beijing CWBIO Biotechnology Co., Ltd. (China). The BCA protein quantification kit and ultrasensitive ECL developer were purchased from Suzhou New Semi Biotechnology Co., Ltd. (China). Anti-phospho-p44/42 MAPK (ERK1/2) antibody (No. 4370) and anti-p44/42 MAPK (ERK1/2) antibody (No. 4695) were purchased from Cell Signaling Technology. Anti-GAPDH (AF1186) were purchased from Shanghai Beyotime Biotechnology Co., Ltd. (China). Anti-mouse IgG HRP-conjugated antibody and anti-rabbit IgG HRP-conjugated antibody were purchased from Cell Signaling Technology. Biotin-labeled goat anti-mouse/rabbit IgG polymer and DAB color development kits were purchased from Beijing Zhongshan Jinqiao Biotechnology Co., Ltd. (China).

2.2 Synthesis of CHI-C and ODex

The syntheses of CHI-C and ODex were similar to the previous synthesis scheme. In brief, CHI-C was synthesized by the EDC activation reaction between the NH_2 group and the carboxyl group. Chitosan was dissolved in 1 N HCl (aq), and the pH was adjusted to 5 using NaOH solution. An appropriate amount of hydrocinnamic acid was added to the above solution. Then, an equal amount of EDC dissolved in DDW and ethanol solution (1 : 1, v/v) was slowly added. The pH value of the mixture solution was adjusted to 4.5 and vigorously stirred at room temperature for 7 h. After the completion of the reaction, the resulting solution was dialyzed in acidified DDW (pH 5.0, HCl) for 3 days and then dialyzed in DDW for 8 hours to remove excess reagents. CHI-C was obtained by freeze-drying. ODex was synthesized by oxidizing dextran (DEX) with a strong oxidant. In short, DEX was dissolved in DDW with vigorous stirring, and sodium periodate solution was added to the above solution. After stirring for 24 hours, the obtained solution was dialyzed in DDW (molecular weight cutoff: 12 000) for 3 days, and ODex was obtained by freeze-drying.

2.3 Formation of CHI-C/ODex hydrogel (CCOD) and CCOD–Tra

CHI-C and ODex were separately dissolved in PBS and mixed to form CCOD. Similarly, a certain volume of Tra solution was added to the CHI-C solution and then quickly mixed with the CHI-C solution to obtain CCOD–Tra, and the concentration of Tra was 0.25 mg ml^{-1}. The gel time was verified using the tube inversion test.

2.4 Injectability, self-healing, morphology and rheological properties of CCOD and CCOD–Tra

The CCOD–Tra mixture was injected using a single-channel needle (diameter: 29 G), CHI-C–Tra and ODex were mixed for approximately 10 s, and then the hydrogel prepolymer was added to the syringe channel and extruded.

The cylindrical hydrogel was cut into two pieces and dyed with different colors. Then, it was pieced together under certain pressure. After 5 minutes, the self-healing ability of the hydrogel was observed.

The microstructure of CCOD and CCOD-BP was lyophilized, and a layer 2 nm thick was sputtered on the surface of the sample to increase its conductivity. The microstructure of the hydrogels was observed under a JEOL FESEM 6700F electron microscope, and the energy of the primary electron was 3 kV.

Similar to the previous test scheme, the cylindrical hydrogel was prepared with a 30 mm diameter and 4 mm height. In all the experiments, the parallel plate geometry diameter was 25 mm, and the temperature of 25 °C, frequency of 0.1 Hz, and oscillatory stress of 1 Pa were kept constant. The self-healing ability of the hydrogel was tested by the rheological test in continuous step strain measurements at a fixed frequency of 10 rad s^{-1}. Each strain interval was kept as 150 s.

2.5 Swelling and degradation of the CCOD and CCOD-BP

A certain amount of hydrogel was placed in a 9 cm Petri dish with PBS, and the hydrogel was removed from the Petri dish and weighed after excess surface water was removed. The swelling rate (SR) is determined by the following formula:

$$\mathrm{SR}\ (\%) = (W_t - W_0)/W_0 \times 100\%$$

The degradation rate (DR) is determined by the following formula:

$$\mathrm{DR}\ (\%) = (W_0 - W_t)/W_0 \times 100\%$$

W_t is the weight of the hydrogel removed from the Petri dish at different time points, and W_0 is the initial weight of the wet hydrogel. The experiment was repeated.

2.6 Biofunctionality of the hydrogels

Fresh pig skin, available from the market, was used to test the adhesion between the hydrogel and host tissue. The skin tissue was fully washed and simply cut into 20 mm × 40 mm rectangles. A certain volume of hydrogel solution was applied to the surface of the pig skin, and the other skin was covered up. The adhesion area was 20 mm × 10 mm and tested with a tensile machine. All these tests were carried out three times.

Hepatic hemorrhage ICR mice (female, weight 20–30 g) were used to test the hemostatic properties of the hydrogels. Briefly, the mice were anesthetized with 4% w/v chloral hydrate and fixed on a surgical board, and the board was tilted approximately 30°. The mouse liver was exposed through an abdominal incision, and the tissue fluid near the liver was wiped with gauze. A preweighed filter paper was placed under the liver, a 2 mm wound was cut on the liver with a scalpel, and CCOD or CCOD–Tra solution was immediately injected into the bleeding site with a syringe. After 10 minutes, the weight of the blood absorbed by the filter paper was compared between the treatment group and the control group (no treatment after liver cut).

A standard curve for Tra was obtained using a UV spectrophotometer. The drug sustained-release curve testing protocol is similar to that reported in the previous article.[37] CCOD–Tra were placed in 24-well plates for drug release studies at 37 °C, with three parallel groups for each sample, then add 1.5 ml of PBS to it and remove 1 ml of PBS from each well at the predetermined time, and then add 1 ml of new PBS. The absorbance at 495 nm was measured by UV spectrophotometer to draw the sustained release curve of Tra.

2.7 Cell culture and osteoclast differentiation

RAW264.7 cells line, obtained from Jilin Provincial Key Laboratory of Tooth Development and Bone Remodeling, were maintained with 5% CO_2 at 37 °C in α-MEM supplemented with 10% (v/v) fetal bovine serum (FBS), 100 U ml^{-1} penicillin and 100 μg ml^{-1} streptomycin.

For differentiation, cells were cultured in α-MEM with 5% FBS, 100 U ml^{-1} penicillin and 100 μg ml^{-1} streptomycin, 50 ng ml^{-1} RANKL and 50 ng ml^{-1} macrophage colony-stimulating factor (MCS-F).

After 5 days of osteoclast differentiation, TRAP-positive cells were detected by TRAP Stain Kit, cells containing three or more nuclei were counted as osteoclasts.

2.8 Live/dead staining and cell counting kit-8

RAW264.7 cells were seeded into 96-well plates at 10 000 cells per well. CCOD and CCOD–Tra (the concentration of Tra was 50 nM, 100 nM and 500 nM) were added to the culture medium, and the cells were incubated at 37 °C for 24 h and 48 h. At each time point, 200 μl AM/PI was added to the wells and incubated at 37 °C in the dark for 15 minutes, then a fluorescence microscope was used for observation.

RAW264.7 cells were inoculated into 96-well plates at 5000 cells per well. CCOD or CCOD–Tra (the concentration of Tra was 50 nM, 100 nM and 500 nM) was added to the culture medium and then incubated at 37 °C for 24 h and 48 h. At each time point, CCK-8 (10 μl) was added to each well and incubated at 37 °C for 1–2 h, then a microplate reader was used to measure the absorbance at 450 nm.

2.9 Reverse transcription-polymerase chain reaction (RT-PCR)

RAW264.7 cells were inoculated into 6-well plates, CCOD and CCOD–Tra were added into the osteoclast differentiation medium and cultured for 5 days. After collecting the cells, total RNA was extracted using the RNA extraction kit and reverse transcribed using the transcription kit. RT-PCR was performed using the SYBR kit, and the primers are shown in Table 1. GAPDH was selected as the internal reference. The reaction conditions were as follows: an initial predenaturation step at 95 °C for 30 s, followed by 40 cycles of denaturation at 95 °C for 5 s and annealing/extension at 60 °C for 30 s. The relative expression levels were calculated by the $2^{-\Delta\Delta C_t}$ method.

2.10 Western blot

We collected RAW264.7 cells, placed the cells on ice in RIPA containing 1% PMSF for 30 min, and then used a BCA protein quantitative kit to measure the protein concentration. Protein of 20 μg was loaded onto 10% SDS-PAGE gels for separation, and then the separated proteins were electroblotted onto a nitrocellulose membrane at 2 h for 200 mA. The membrane

Table 1 Primer sequences for RT-PCR

Gene	Primer sequence (5′–3′)
MMP-9	F: CAAAGACCTGAAAACCTCCAAC
	R: GACTGCTTCTCTCCCATCATC
C-FOS	F: CGGGTTTCAACGCCGACTA
	R: TTGGCACTAGAGACGGACAGA
TRAP	F: CAAGAACTTGCGACCATTGTTA
	R: ATCCATAGTGAAACCGCAAGTA
GAPDH	F: AGGTCGGTGTGAACGGATTTG
	R: TGTAGACCATGTAGTTGAGGTCA

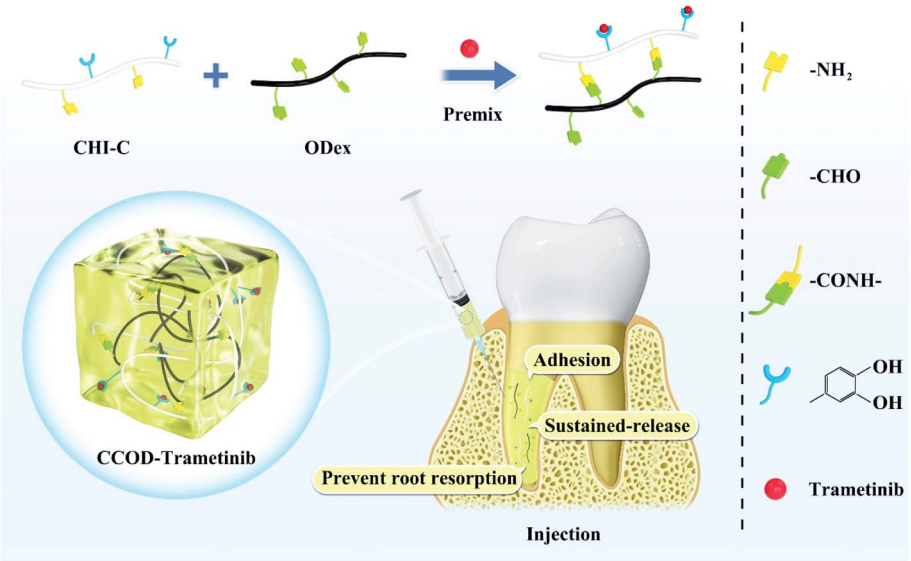

Scheme 1 A schematic diagram of the design strategy and application of the bio-multifunctional CCOD–Trametinib hydrogel for preventing root resorption.

was blocked with 5% bovine serum albumin (BSA) for 1 h at 4 °C and incubated with primary antibodies at 4 °C overnight. After washing with Tris-buffered saline containing 0.05% Tween-20 (0.05% TBST buffer), the membrane was incubated with HRP-conjugated secondary antibodies. Then, the membrane was washed with TBST and reacted with enhanced chemiluminescence (ECL) for protein band visualization. The intensities of the bands were analyzed by ImageJ (Fujifilm, Tokyo, Japan). The relative protein expression was calculated by normalization to GAPDH. The following primary antibodies were used: ERK1/2 (1 : 1000), p-ERK1/2 (1 : 1000) and GAPDH (1 : 1000).

2.11 Establishment of a rat OTM model

This experiment used 20 SD rats aged 6 weeks (male, 200–220 g). All animal procedures were approved by the Experimental Animal Welfare Ethics Committee of Jilin University (KT202003139). The animals were randomly divided into 4 groups with 5 rats in each group. Group A: OTM group (OTM treatment, injected PBS 20 μl per day), Group B: CCOD group (OTM treatment, injected CCOD 20 μl on the first day), Group C: Tra group (OTM treatment, injected Tra 0.05 mg per kg per day in 20 μl), Group D: CCOD–Tra group (OTM treatment, injected CCOD–Tra 0.25 mg kg^{-1} on the first day in 20 μl).

The animal experiments were performed using a previously described method.[38,39] The rat OTM modeling process is as follows: fix one end of the orthodontic nickel–titanium tensile spring on the upper first molar of the anesthetized rat, and the other end is connected to the incisor. Photosensitive resin is used to prevent equipment from falling off (Fig. 4a). Tensile spring pulls the first molar to move mesially, with a force of 50 g, and the treatment lasted for 14 days. Rats were given local injection by the insulin syringe, and the injection site was the periodontal tissue surrounding the roots of maxillary first molars. The rats in the OTM and Tra groups were given drug treatment once a day, and the rats in the CCOD and CCOD–Tra groups were given drug only on the first day. After being injected into the periodontal tissue, due to the characteristic of temperature sensitivity and high adhesiveness, CCOD and CCOD–Tra were coagulated into a hydrogel, adhered to the periodontal tissue (Fig. 4b). On the 14th day, all rats were euthanized, and the upper jaws of the rats were dissected and fixed in 4% paraformaldehyde (PFA) for 24 hours (Scheme 1).

2.12 Measurement of tooth movement distance

After 14 days of OTM treatment, Micro CT (HiScan XM Micro CT) was used to scan the rats' maxillary alveolar bones. The scanning parameters were as follows: 80 kV, 100 μA, single exposure time 50 ms, scanning resolution 25 μm, scanning angle interval 0.5 degrees. The reconstruction and analysis software was AMIRA. The movement distance of the rat maxillary first molar was measured by the micro-CT, the measurement range was the crown distances between the first molar and second molar (Fig. 4c).

2.13 Assessment of OIIRR

Same as previous research, the assessment of OIIRR was measured by micro-CT.[40,41] The detection was performed on the coronal plane slice of the mesial root of the maxillary first molar. The outer and inner boundaries of the mesial root were determined from the cementoenamel junction to the root apex (Fig. 4e). The resorption lacunae volume (RLV) and total root volume (TRV) were determined by AMIRA software. The width and depth measurements of the lacuna were measured and the TRV was calculated by adding the remaining and resorption root volume (Fig. 4f). The ratio of the RLV to the TRV was the percentage of root resorption (PRR).

2.14 Histological examination

The samples fixed with 4% PFA were decalcified in 10% ethylenediamine tetraacetic acid (EDTA) for 12 weeks. After dehydration with an ethanol gradient, the samples were embedded in paraffin and sectioned at a thickness of 3 μm. The sections were stained with hematoxylin–eosin (H&E) staining solution and observed under a microscope. TRAP staining was used to identify the osteoclasts on the tooth root surface in the sections. Three areas were randomly selected in each sample, TRAP-positive cells were counted, and the average value was calculated.

2.15 Immunohistochemistry (IHC)

After heating and dewaxing, the sections were placed into 1% sodium citrate buffer at 62 °C overnight for antigen retrieval, and then 100 μl 3% hydrogen peroxide was added to each section and incubated at room temperature in the dark for 15 minutes. After washing 3 times with phosphate buffer saline (PBS), blocking solution was added for blocking at 37 °C for 1 hour, and then the sections were incubated with primary antibody at 4 °C for 12 h. The primary antibody was diluted with PBS at the following concentrations: anti-MMP-9 (1 : 500), anti-C-FOS (1 : 500). After rinsing, the sections were incubated with biotin-labeled goat anti-mouse/rabbit IgG polymer secondary antibody for 2 h. Then, DAB chromogen was used to develop the color, and a microscope was used for observation. Three fields were selected at random, and the positive cells were counted by ImageJ.

2.16 Statistical analysis

The data are expressed as the mean ± standard deviation. Comparisons between two groups were performed with the two-way *t*-test, and comparisons among multiple groups were performed with one-way ANOVA followed by Bonferroni *post hoc* tests. P values <0.05 were considered significant.

3. Results and discussion

3.1 Material synthesis and verification of related characterizations

Similar to in previous work,[36] CHI-C and ODex were synthesized to prepare a bio-multifunctional gel. CHI-C was obtained by EDC chemistry to graft hydrocaffeic acid onto chitosan, and the grafting density was approximately 20%, which was confirmed by proton nuclear magnetic resonance spectroscopy (1H NMR) and ultraviolet-visible (UV-vis; Fig. S1, ESI†). ODex was obtained by oxidizing hydroxyl groups with sodium periodate, a strong oxidant, and the degree of oxidation density was approximately 35%, which was verified by the hydroxylamine hydrochloride method, 1H NMR and Fourier transform infrared (FT-IR) spectroscopy (Fig. S2, ESI†).

CHI-C and ODex were used as the main backbones of the gel, and Schiff's base bonds were used as the gel forming mechanism to synthesize the carrier gel. First, ODex and CHI-C were dissolved in PBS, the concentration of ODex was 0.008 and the concentration of CHI-C was 0.032, and then 10 μl DMSO loaded with Tra was added to 1 ml CHI-C. The sustained release cycle of Tra was extended with the help of dopamine. After full mixing, CHI-C with Tra was blended with ODex to form CCOD–Tra. The tube inversion test in Fig. 1a confirmed the cross-linking of the hydrogel. The gelation time was approximately 10 s, and the gelation time did not change significantly with the addition of Tra. The gel microstructure and storage modulus of CCOD and CCOD–Tra also had no obvious change. The FT-IR spectra in Fig. 1b showed that CCOD–Tra had a characteristic peak of Tra at 1720 cm^{-1}, which proves the successful drug loading, and the theoretically Tra loading efficiency is about 100%. Meanwhile, with the increase of gel crosslinking density, the sustained release period of CCOD was significantly prolonged, we chose a gel with a total mass fraction of 2% as the drug-loaded gel, and the sustained-release period was about 20 days, which met the treatment time requirement (Fig. 1c).

In the process of local drug delivery, with the assistance of dopamine and aldehyde groups, the gel could stay in the periodontal area for a long time and reduce periodontal bleeding. To better test the biological characteristics of CCOD–Tra, we added different dyes to the hydrogel for distinct observations, cut the hydrogel into two pieces, and then placed them back together, and it was observed that the gel repaired itself within 3 minutes in Fig. 1f. The results showed that the hydrogel had good self-healing ability. We further evaluated the self-healing ability through rheological shear recovery tests. For the results shown in Fig. 1g and h, the continuous shear strain alternated between 1% and 300%, and the stress of each segment was maintained for 150 seconds. At a low shear strain of 1%, the hydrogel structure was stable, and G' was significantly higher than G''. At a higher shear strain of 300%, the hydrogel had shear thinning characteristics, and G'' was higher than G'. G' and G'' changed synchronously with the alternating strain. This process was repeatable, which proved that the hydrogel had excellent self-healing ability. Similar to other hydrogels using amide bonds as the gel forming mechanism, CCOD is injectable, which facilitated the administration operation. It could be injected directly through a syringe (29 G) and could adhere directly to the injected area after injection.

We then aimed to more intuitively evaluate the adhesion ability of CCOD–Tra and its ability to reduce periodontal bleeding. We first used a lap shear test on pigskin to evaluate the adhesion ability of CCOD–Tra in Fig. 1d. The results showed that the adhesion strength of CCOD was approximately 30 kPa, which was approximately 8 times than that of fibrin glue. With the addition of Tra, the adhesion strength was slightly reduced, to approximately 25 kPa, because the drug may occupy a small amount of the gel functional groups. We then established a rat liver injury model. The blood loss of the CCOD and CCOD–Tra groups was only 27 and 25 mg, respectively, while that of the control group without any intervention was 193 ± 4 mg, indicating that the hydrogel has excellent hemostatic ability in Fig. 1e. CCOD and CCOD–Tra achieved even better hemostasis than fibrin glue (56 ± 14 mg), which is commonly used in clinical practice.

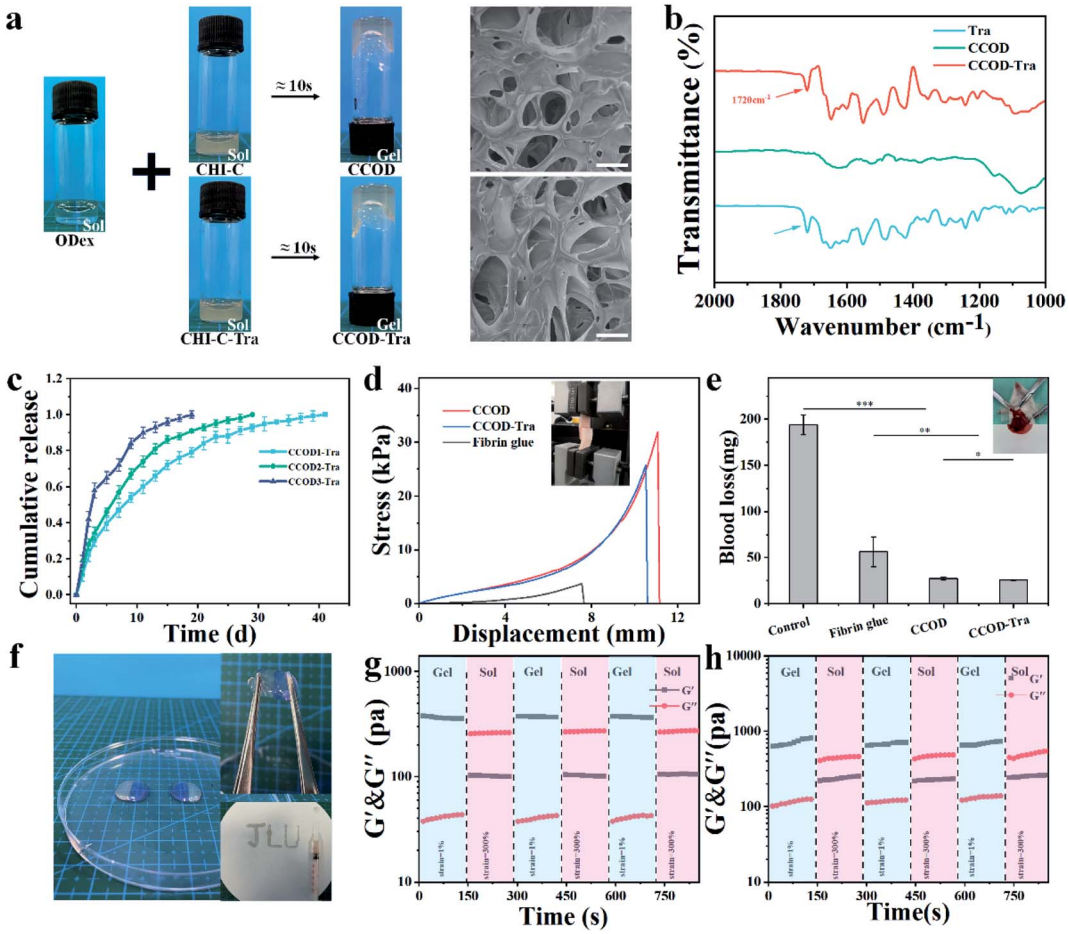

Fig. 1 Bio-malformation and characterization of CCOD and CCOD–Tra. (a) The photo of CCOD and CCOD–Tra obtained by a tube inversion test. SEM images of the CCOD and CCOD–Tra. Scale bar: 50 μm. (b) The FT-IR spectra showed the formation of the CCOD and CCOD–Tra. (c) Cumulative Tra release curve. CCOD1–Tra, CCOD2–Tra, CCOD3–Tra indicated that the total mass fraction of gel was 1%, 2%, 3%. (d) Typical stress–displacement curve of CCOD and CCOD–Tra bonded pigskin. Illustration: photo of the hydrogel adhered to the surface of pig skin that simulates human skin. (e) Hemostatic performance of CCOD and CCOD–Tra. Illustration: Liver Scratch Modeling. (f) The self-healing process of two semi-circular hydrogels of different colors after 5 minutes; the injection process of the mixed hydrogel. CCOD–Tra can be injected with a needle (29 G) and JLU was drawn with the needle. (g and h) G' and G'' values of the CCOD and CCOD–Tra in continuous step strain measurements (a fixed frequency of 10 rad s^{-1}. Each strain interval was kept as 150 s).

3.2 Biocompatibility of the CCOD and CCOD–Tra

It is important to verify the biocompatibility of biomaterials, and we used live/dead staining and CCK-8 experiments to evaluate the cytotoxicity of CCOD and CCOD–Tra. The results of the live/dead staining experiment showed that the survival rate of RAW264.7 cells cocultured with CCOD and CCOD–Tra for

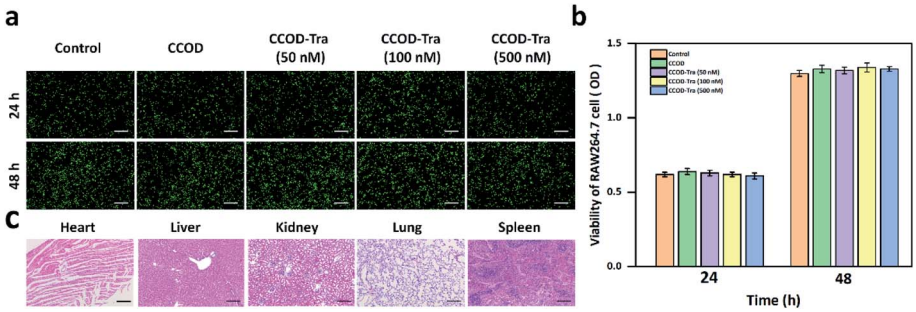

Fig. 2 Bio-multifunction and bio-compatibility of CCOD and CCOD–Tra. (a) Live/dead staining of RAW264.7 cells at 24 h, 48 h. Scale bar: 200 μm. (b) Cytotoxicity of the CCOD and CCOD–Tra evaluated by CCK-8. *: $P < 0.05$, **: $P < 0.01$. (c) H&E staining of hearts, livers, kidneys, lungs and spleens in the CCOD–Tra group. The scale bar is 200 μm.

24 h and 48 h exceeded 90%, and there was no difference from that of the control group (Fig. 2a). The CCK-8 results showed that the proliferation rates of RAW264.7 cells in the CCOD group and CCOD–Tra groups were not different from that in the control group at 24 and 48 h (Fig. 2b). We also evaluated the organs of rats in the CCOD–Tra group by H&E staining, and there was no obvious abnormalities in the heart, liver, spleen, lung or kidney (Fig. 2c). These results indicated that CCOD–Tra had good biocompatibility both *in vivo* and *in vitro*.

3.3 CCOD–Tra inhibits the differentiation of osteoclast by blocking ERK1/2 signaling pathway

During the OTM, force induces osteoclast differentiation, osteoclasts attached to the cementum surface caused OIIRR.[4,6] In the osteoclast differentiation, RANKL is a key factor binding to the RANK receptor,[9–11] then the intracellular domain of RANK will recruit TRAF6 to activate downstream signaling molecules like NF-kB, MAPK, *etc.*, which initiate the expression of genes like TRAP, C-FOS and MMP-9 in the nucleus, so the osteoclasts were differentiated.[18–20]

To verify the effect of CCOD–Tra on adjusting osteoclast differentiation, we induced RAW264.7 cells by RANKL coculturing with CCOD–Tra for 5 days, then determined the number of mature osteoclasts by TRAP staining. The results indicated that under the induction of RANKL, RAW264.7 cells were differentiated into mature osteoclasts, however, 100 nM and 500 nM CCOD–Tra treatment significantly suppressed the differentiation of osteoclasts induced by RANKL (Fig. 3a). We also monitored the mRNA expression levels of TRAP, MMP-9 and C-FOS in RAW264.7 cells, qPCR results showed that, the expression levels of TRAP, MMP-9 and C-FOS were significantly increased by the stimulation of RANKL, but down-regulated by the treatment of 100 nM and 500 nM CCOD–Tra (Fig. 3b).

As a classic member of the MAPK family, it was found that ERK1/2 signaling pathway played an important role in regulating the differentiation of osteoclasts. To verify whether the regulatory effect of CCOD–Tra on the expression of osteoclast-related factors depended on ERK1/2 signaling pathway, we induced RAW264.7 cells by RANKL cocultured with CCOD–Tra for 5 days, then detected the protein expression levels of p-ERK1/2 and ERK1/2 in RAW264.7 cells by western blot. Results showed that the stimulation of RANKL significantly increased the expression level of p-ERK1/2, but 100 nM and 500 nM CCOD–Tra reversed this situation (Fig. 3c). These results indicated that CCOD–Tra significantly inhibited osteoclast differentiation induced by RANKL *via* blocking the ERK1/2 signaling pathway, which suggests that CCOD–Tra may prevent OIIRR by inhibiting the maturation and differentiation of osteoclasts.

3.4 Effects of CCOD–Tra on tooth movement

In order to verify whether CCOD–Tra can prevent OIIRR, we established a rat OTM model, and periodontal injected drugs to treat rats. After 14 days, we first measured the tooth moving distance of the maxillary first molar by micro-CT. In the OTM

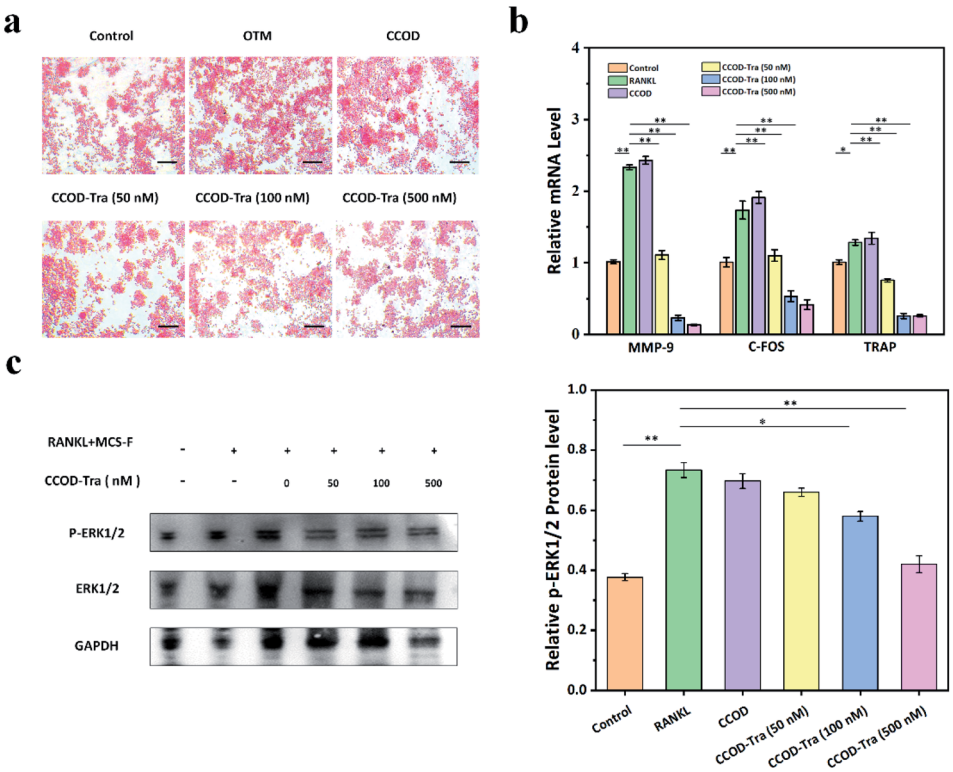

Fig. 3 TRAP staining, mRNA and protein expression levels of RAW264.7 cells. (a) TRAP staining of RAW264.7 cells. Scale bar: 200 μm. (b) mRNA expression levels of MMP-9, C-FOS and TRAP were determined by qPCR. (c) Western blotting of p-ERK1/2, ERK1/2 and GAPDH. *: $P < 0.05$, **: $P < 0.01$.

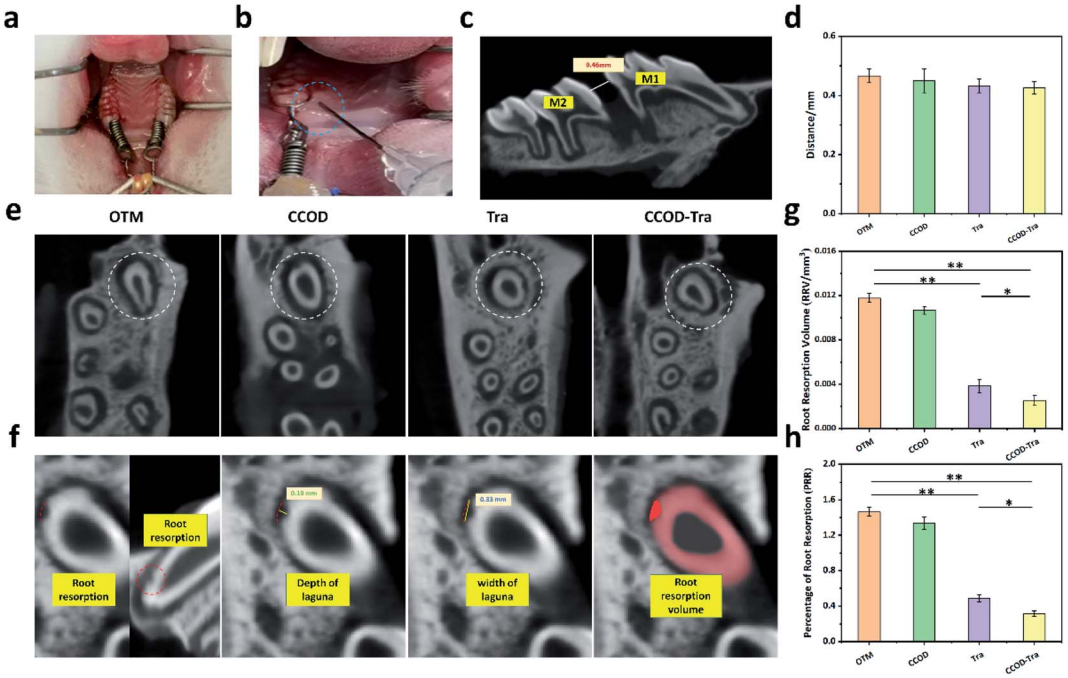

Fig. 4 The establishment of a rat OTM model and the measurement of tooth moving distance and root resorption volume. (a) The establishment of a rat OTM model. (b) CCOD–Tra was injected into the periodontal tissue, and then adhered to the periodontal tissue (blue circle). (c) The micro-CT images were used to measure tooth moving distance, M1 is the maxillary first molar, M2 is the second molar. (d) The distance of tooth moving. (e) Root resorption lagunas on the mesial root of maxillary first molars (white circles). (f) Demonstration of root resorption measurements by micro-CT images. (g) Quantitative analysis of RRV determined by micro-CT images. (h) Quantitative analysis of PRR determined by micro-CT images. *: $P < 0.05$, **: $P < 0.01$.

group, the tooth moving distance was 0.45 ± 0.024 mm, which was consistent with the results obtained in previous studies.[42] The distance in CCOD group was 0.45 ± 0.043 mm, there was no significant difference from the control group. However, in the Tra and CCOD–Tra groups, the distance was slightly smaller than that in the OTM group, which were 0.44 ± 0.022 mm and 0.43 ± 0.013 mm (Fig. 4d). These results showed that CCOD had no effect on the OTM distance while Tra and CCOD–Tra had a slight inhibitory on OTM.

3.5 Effects of CCOD–Tra on preventing OIIRR

In order to quantify the effect of CCOD–Tra on preventing OIIRR, micro-CT was used to measure the RLV and TRR of rats in each group, and the PRR reflected the degree of root resorption. Then we found that the PRR of the Tra and CCOD–Tra groups was significantly lower than that of the OTM group, while the PRR of the CCOD–Tra group was also lower than that of the Tra group (Fig. 4g and h). These results showed that both Tra and CCOD–Tra prevented OIIRR, but the effect of CCOD–Tra was better. CCOD–Tra had the advantages of both CCOD and Tra, it adhered to the periodontal tissue and released Tra sustained, so that the local drug kurtosis was maintained continuously, which was better to prevent OIIRR.

3.6 Histological changes induced by CCOD–Tra

H&E, TRAP and IHC staining were carried out to detect the histological changes in the periodontal of rats. Consistent with micro-CT results, H&E staining showed that in the OTM group, a large number of bone resorption lacunas (Fig. 5a, indicated by the blue arrows) were seen on the surface of tooth root and alveolar bone, the depth of the lacunae reached the dentin. Compared with OTM group, the number of resorption lacunae in Tra and CCOD–Tra groups was significantly reduced (Fig. 5a), and the depth was shallow, suggesting that both Tra and CCOD–Tra can prevented OIIRR. Notably, in the CCOD–Tra group, the number of resorption lacunae was lower and the depth was shallower in comparison with that in the Tra group, which indicated that CCOD–Tra was more effective in preventing the OIIRR.

Studies have shown that OIIRR was caused by the osteoclasts,[3] to further quantify the osteoclasts, we performed TRAP staining to explore the effect of CCOD–Tra on osteoclast differentiation. TRAP-positive cells located on the mesial side of the rats' maxillary first molar were quantified (Fig. 5a, indicated by the red arrows). The number of TRAP-positive cells was counted in three fields of view. In OTM group, there was a large number of TRAP-positive cells on the surface of cementum and alveolar bone, showing that the OTM force induced the differentiation of osteoclast. In the Tra group, the number of TRAP-positive cells was significantly decreased when compared with the OTM group, and in the CCOD–Tra group the TRAP-positive cells' number was almost zero (Fig. 5b). These results indicated that both Tra and CCOD–Tra had a positive effect on inhibiting osteoclast differentiation but the treatment of CCOD–Tra was better.

To verify whether the CCOD–Tra prevented OIIRR was related to the expression of MMP-9 and C-FOS, we evaluated the

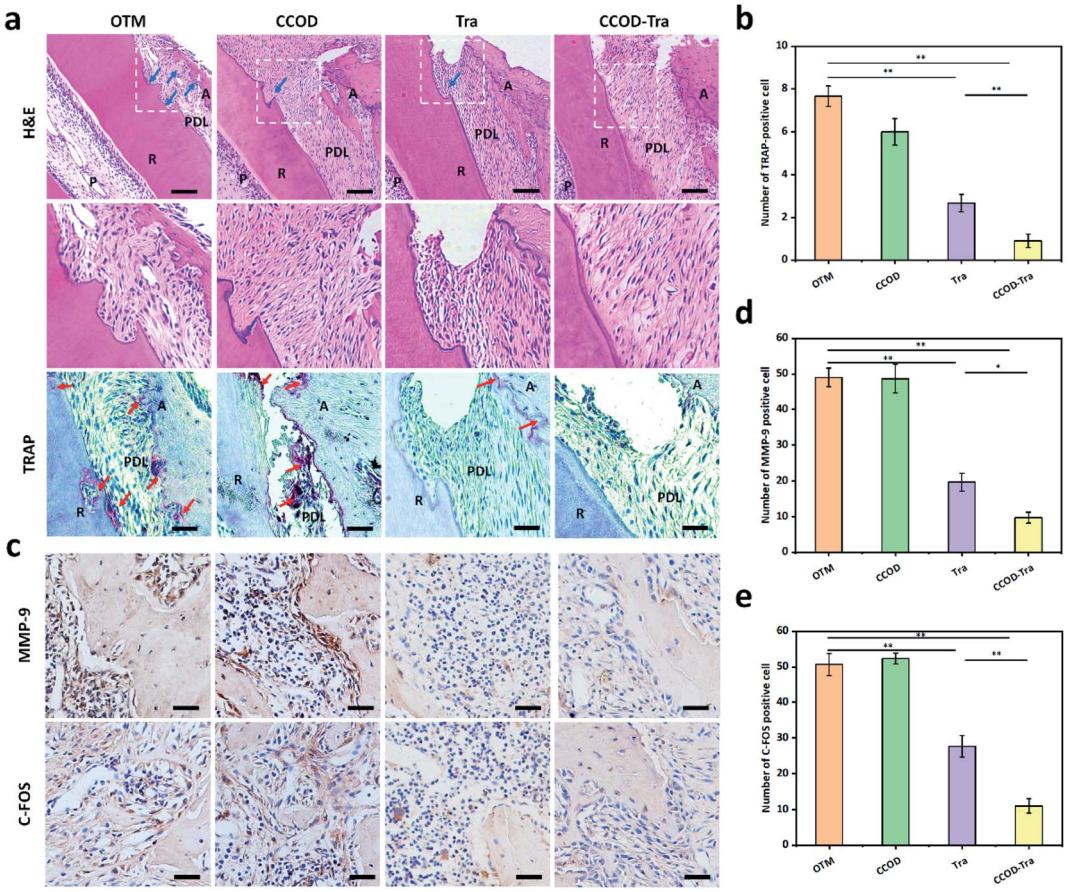

Fig. 5 Histological changes induced by CCOD–Tra. (a) H&E and TRAP staining of the maxillary of rats. The root resorption lacunas were pointed by the blue arrows. The TRAP-positive cells were pointed by the red arrows. Scale bar of H&E staining: 200 μm, scale bar of TRAP staining: 100 μm. (b) TRAP positive cells were quantified by counting the numbers in three visual fields, and then the average values were calculated. (c) IHC staining. Scale bar: 50 μm. (d) MMP-9 positive cells were counted and the averaged values were calculated. (e) C-FOS positive cells were counted and the averaged values were calculated. *: $P < 0.05$, **: $P < 0.01$.

number of MMP-9- and C-FOS-positive cells by IHC. Three visual fields in the area were selected for evaluation, and the average value was obtained (Fig. 5c–e). In the OTM and CCOD groups, the number of MMP-9- and C-FOS-positive cells was large, and the OIIRR in these two groups was severe. But in the Tra and CCOD–Tra groups, the number of MMP-9- and C-FOS-positive cells was smaller, and in the CCOD–Tra group, the positive cells were also fewer than those in Tra group, which suggesting that CCOD–Tra was more effective than Tra in preventing OIIRR by limiting the differentiation of osteoclasts in periodontal tissue. CCOD–Tra had the advantages of high adhesion and sustained-release of Tra, so the effect of preventing OIIRR was stronger than that of Tra.

4. Conclusion

In summary, we have developed a bio-multifunctional hydrogel that can be combined with Trametinib to form a CCOD–Tra hydrogel to prevent OIIRR effectively. When injected locally, CCOD–Tra was adhere to the periodontal tissue, and sustained-release Tra. CCOD–Tra is convenient to administer and has high biocompatibility. The high adhesion of CCOD provided a good biological environment that could maintain the concentration of the drug at a therapeutic level to maximize its efficacy, and CCOD–Tra was therefore more effective than Tra treatment. It is worth noting that at the molecular level, CCOD–Tra could reduce the expression of TRAP, MMP-9 and C-FOS, thereby effectively inhibiting the differentiation of osteoclasts and preventing OIIRR, and the effect was mediated by the ERK1/2 signaling pathway. In summary, we believe that Tra could be used as an effective drug to prevent OIIRR, and CCOD–Tra could provide a good option for future clinical treatment and prevention of OIIRR. It is possible to improve the adverse side effects of orthodontic treatment and broaden the indications for orthodontia.

Conflicts of interest

The authors declare no competing financial interest.

Acknowledgements

This work was supported by the National Natural Science Foundation of China (No. 81801005, 201870795, 21774043,

21975098, 51905526), Health Commission of Jilin Province No. 2018-33-05 and Natural Science Foundation of Jilin Province, No. 20200201344JC, the Fundamental Research Funds for the Central Universities (JLU) and the Program for JLU Science and Technology Innovation Research Team (No. 2017TD-06).

References

1 S. Henneman, J. W. Von den Hoff and J. C. Maltha, *Eur. J. Orthod.*, 2008, **30**, 299–306.
2 B. Melsen, *Angle Orthod.*, 1999, **69**, 151–158.
3 L. Feller, R. A. G. Khammissa, G. Thomadakis, J. Fourie and J. Lemmer, *BioMed Res. Int.*, 2016, **2016**, 4864195.
4 M. Motokawa, T. Sasamoto, M. Kaku, T. Kawata, Y. Matsuda, A. Terao and K. Tanne, *Eur. J. Orthod.*, 2012, **34**, 350–356.
5 B. Weltman, K. W. L. Vig, H. W. Fields, S. Shanker and E. E. Kaizar, *Am. J. Orthod. Dentofac. Orthop.*, 2010, **137**, 462–476.
6 C. Lu, L. Chen and Y. Hua, *Ann. Transl. Med.*, 2019, **7**, 787.
7 J. B. Tyrovola, M. N. Spyropoulos, M. Makou and D. Perrea, *J. Oral Sci.*, 2008, **50**, 367–376.
8 P. Brudvik and P. Rygh, *Eur. J. Orthod.*, 1995, **17**, 177–188.
9 M. A. Zinnia and A. B. M. M. Khademul Islam, *Int. J. Biol. Macromol.*, 2021, **186**, 351–364.
10 D. Nishida, A. Arai, L. Zhao, M. Yang, Y. Nakamichi, K. Horibe, A. Hosoya, Y. Kobayashi, N. Udagawa and T. Mizoguchi, *Sci. Rep.*, 2021, **11**, 4575.
11 L. Zhou, J. Wang, J. Zhao, F. Kuai and H. Yang, *Am. J. Transl. Res.*, 2020, **12**, 8099–8110.
12 M. Wu, Y. Wang, L. Deng, W. Chen and Y.-P. Li, *Int. J. Biol. Sci.*, 2012, **8**, 1398–1407.
13 Z. Yao, W. Lei, R. Duan, Y. Li, L. Luo and B. F. Boyce, *J. Biol. Chem.*, 2017, **292**, 10169–10179.
14 X. Ma, J. Liu, L. Yang, B. Zhang, Y. Dong and Q. Zhao, *Life Sci.*, 2018, **209**, 140–148.
15 K. Sun, J. Zhu, Y. Deng, X. Xu, F. Kong, X. Sun, L. Huan, C. Ren, J. Sun and J. Shi, *Front. Pharmacol.*, 2021, **12**, 629968.
16 X. Lin, G. Yuan, Z. Li, M. Zhou, X. Hu, F. Song, S. Shao, F. Fu, J. Zhao, J. Xu, Q. Liu and H. Feng, *J. Cell. Physiol.*, 2020, **235**, 5951–5961.
17 X. Xu, R. Wang, R. Wu, W. Yan, T. Shi, Q. Jiang and D. Shi, *FASEB J.*, 2020, **34**, 8402–8415.
18 B. Kim, K. Y. Lee and B. Park, *Phytomedicine*, 2018, **51**, 181–190.
19 W. Feng, H. Liu, T. Luo, D. Liu, J. Du, J. Sun, W. Wang, X. Han, K. Yang, J. Guo, N. Amizuka and M. Li, *Sci. Rep.*, 2017, **7**, 41411.
20 W. Wang, M. Huang, Y. Hui, P. Yuan, X. Guo and K. Wang, *J. Cell. Biochem.*, 2019, **120**, 7333–7340.
21 X. Lu, Y. Ito, P. Atsawasuwan, S. Dangaria, X. Yan, T. Wu, C. A. Evans and X. Luan, *Bone*, 2013, **54**, 157–168.
22 T. Lian, C. Li and H. Wang, *Cancer Treat. Rev.*, 2019, **81**, 101907.
23 S. Chen, H. Xu, P. Ye, C. Wu, X. Ding, S. Chen, H. Zhang, Y. Zou, J. Zhao, S. Le, J. Wu, S. Chen and J. Xia, *Int. Immunopharmacol.*, 2020, **80**, 106152.
24 J. de la Croix Ndong, D. M. Stevens, G. Vignaux, S. Uppuganti, D. S. Perrien, X. Yang, J. S. Nyman, E. Harth and F. Elefteriou, *J. Bone Miner. Res.*, 2015, **30**, 55–63.
25 T. Yamaguchi, R. Kakefuda, A. Tanimoto, Y. Watanabe and N. Tajima, *Inflammation Res.*, 2012, **61**, 445–454.
26 S. Huang, F. Yu, Y. Cheng, Y. Li, Y. Chen, J. Tang, Y. Bei, Q. Tang, Y. Zhao, Y. Huang and Q. Xiang, *Front. Pharmacol.*, 2021, **12**, 678322.
27 W. Peng, S. Ren, Y. Zhang, R. Fan, Y. Zhou, L. Li, X. Xu and Y. Xu, *Front. Bioeng. Biotechnol.*, 2021, **9**, 668428.
28 S. Zang, R. Mu, F. Chen, X. Wei, L. Zhu, B. Han, H. Yu, B. Bi, B. Chen, Q. Wang and L. Jin, *Mater. Sci. Eng., C*, 2019, **99**, 919–928.
29 J. Z. Xing, L. Lu, L. D. Unsworth, P. W. Major, M. R. Doschak and N. R. Kaipatur, *Acta Biomater.*, 2017, **49**, 306–315.
30 S. Asefi, M. Seifi, G. H. Fard and A. Lotfi, *Dent. Res. J.*, 2018, **15**, 40–49.
31 Š. Zupančič, L. Casula, T. Rijavec, A. Lapanje, M. Luštrik, A. M. Fadda, P. Kocbek and J. Kristl, *J. Controlled Release*, 2019, **316**, 223–235.
32 J. Tan, M. Zhang, Z. Hai, C. Wu, J. Lin, W. Kuang, H. Tang, Y. Huang, X. Chen and G. Liang, *ACS Nano*, 2019, **13**, 5616–5622.
33 B. Wang, H. E. Booij-Vrieling, E. M. Bronkhorst, J. Shao, P. H. J. Kouwer, J. A. Jansen, X. F. Walboomers and F. Yang, *Acta Biomater.*, 2020, **116**, 259–267.
34 X.-T. He, X. Li, Y. Xia, Y. Yin, R.-X. Wu, H.-H. Sun and F.-M. Chen, *Acta Biomater.*, 2019, **88**, 162–180.
35 X. Xu, Z. Gu, X. Chen, C. Shi, C. Liu, M. Liu, L. Wang, M. Sun, K. Zhang, Q. Liu, Y. Shen, C. Lin, B. Yang and H. Sun, *Acta Biomater.*, 2019, **86**, 235–246.
36 X. Tang, X. Wang, Y. Sun, L. Zhao, D. Li, J. Zhang, H. Sun and B. Yang, *Adv. Funct. Mater.*, 2021, **31**, 2105718.
37 S. Huang, H. Liu, S. Huang, T. Fu, W. Xue and R. Guo, *Carbohydr. Polym.*, 2020, **246**, 116650.
38 E. J. Lira dos Santos, A. B. de Almeida, M. B. Chavez, C. R. Salmon, L. S. Mofatto, M. B. Camara-Souza, M. H. Tan, T. N. Kolli, F. F. Mohamed, E. Y. Chu, P. D. Novaes, E. C. A. Santos, K. R. Kantovitz, B. L. Foster and F. H. Nociti, *Bone*, 2021, **153**, 116139.
39 X. Zhang, Z. Li, Z. Zhao, Y. Chen, Y. Sun and Q. Cai, *Int. Immunopharmacol.*, 2021, **100**, 107991.
40 H. Baser Keklikci and A. Yagci, *Am. J. Orthod. Dentofac. Orthop.*, 2021, **159**, e245–e251.
41 T. Ozturk and N. Gul Amuk, *Lasers Med. Sci.*, 2020, **35**, 1419–1429.
42 J. Chang, P.-J. Chen, E. H. Dutra, R. Nanda and S. Yadav, *Eur. J. Orthod.*, 2019, **41**, 601–608.